

Laser-Induced Fluorescence Instrument for the Detection of Tropospheric OH Radicals

Yutaka Matsumi,* Mitsuhiko Kono,# Toshio Ichikawa, Kenshi Takahashi and Yutaka Kondo†

Solar-Terrestrial Environment Laboratory and Graduate School of Science, Nagoya University, 3-13, Honohara, Toyokawa 442-8507

†Research Center for Advanced Science and Technology, The University of Tokyo, 4-6-1 Komaba, Meguro-ku, Tokyo 153-8904

(Received September 21, 2001)

An instrument for the measurement of troposphric OH radical concentrations using a laser-induced fluorescence technique has been developed. Ambient air is expanded through a pinhole into a low-pressure fluorescence cell and irradiated by the second harmonic of a dye laser at a high repetition rate of 1 kHz. The OH radicals are electronically excited using $A^2\Sigma^+(v' = 0) \leftarrow X^2\Pi(v'' = 0)$ transitions around 308 nm. The fluorescence from OH radicals is collected by a lens system and detected by a photomultiplier. The photoelectron pulses from the photomultiplier are processed by a photon-counting system. The dynode gate of the photomultiplier and counting gate systems are made to minimize the detection of the chamber and Rayleigh scattering signal. The sensitivity of the developed instrument is calibrated with two methods: one is a long-path absorption technique and the other is a titration technique with simultaneous photolysis of water vapor and oxygen. It is found that the background signal is mainly produced by after-pulse effects in the photomultiplier for the fluorescence detection with a dynode gate system. The minimum detection limit is determined to be 7.0×10^5 molecules cm^{-3} for OH radicals with a signal-to-noise ratio of 2 and a signal integration time of 60 s.

The hydroxyl radical (OH) is the most important oxidant in the atmosphere. It is involved in nearly every aspect of atmospheric chemistry through reactions with CO, CH_4, O_3, NO_2, SO_2, and numerous non-methane hydrocarbons.[1–4] Consequently, measurements of OH are necessary to verify the understanding of many atmospheric chemistry processes. Because OH is very reactive, while its ambient concentration is very low (typically$\sim10^6$ molecules cm^{-3}), measurements of OH have proven to be very difficult.[5] Although several research groups have been developing measurement systems for OH radicals in the atmosphere for many years,[6–12] only recently have reliable measurements for OH radicals in the troposphere been obtained.[13–20]

Several techniques for the detection of atmospheric OH radicals have been developed.[5] The long path absorption techniques for OH measurements in the ultraviolet (UV) region have been reported.[20–24] Not only OH molecules but also other species have absorptions in the wavelength region used in absorption measurements, a few tenths of nm near 308 nm. Absorbing species that have been identified are SO_2, CH_2O, CS_2, and naphthalene. Absorption bands due to as yet unidentified compounds are also present. In the ion-assisted mass spectroscopy method,[16,25,26] isotopically labeled $^{34}SO_2$ is added near the atmospheric sampling inlet. In the presence of H_2O vapor, the SO_2 reacts with ambient OH molecules to form H_2SO_4. The sulfuric acid concentration is then determined by reacting it with $NO_3^-\cdot HNO_3$ ions in a flow tube and measuring the HSO_4^-/NO_3^- ratio with the mass spectrometer. The method is capable of adequate sensitivity for ambient OH measurements and has been used in the field. A technique using oxidation of isotopically labeled ^{14}CO was also developed.[27] The rate of removal of the CO, observed through measurement of the radioactivity from the $^{14}CO_2$ product, was used to determine the ambient OH concentration. Although this method is absolute, requiring no calibration other than the OH + CO reaction rate coefficient, the usage of the radioactive ^{14}CO is not suitable for common applications.

In this paper, we report the development of an OH instrument based on a laser-induced fluorescence (LIF) technique. In the LIF detection of tropospheric OH radicals, the most difficult problem arises from laser-generated OH.[5] Just like solar radiation, the laser light photolyzes ozone molecules, whose concentration in ambient air is 2–4 order larger than that of the OH radicals, and then produces $O(^1D)$ atoms which react with water vapor to form OH in the path of the laser beam:

$$O_3 + h\nu(\text{laser}) \rightarrow O_2 + O(^1D) \quad (1)$$

$$O(^1D) + H_2O \rightarrow 2OH. \quad (2)$$

Such spurious OH radicals absorb another photon during the same laser pulse and fluoresce. A number of techniques have been introduced to reduce the ozone interferences.[6,7,28,29] i) One of the most notable techniques is the sampling of ambient

Current address: Atomic and Molecular Physics Laboratory, Research School of Physical Science and Engineering, The Australian National University, Canberra, ACT 0200, Australia

air at low pressure through a small inlet. This technique is called FAGE (Fluorescent Assay by Gas Expansion). The sample air containing OH in atmospheric pressure is expanded through a nozzle into the fluorescence cell and then pumped by a high-speed pump, so that detection is performed at pressures of a few hundred Pa. Under these reduced pressure conditions, the rates of the collisional quenching processes of the OH laser-excited state become comparable to its radiative rate of 1.4 μs^{-1}. Therefore, the fluorescence persists for a significant time beyond the 5 to 15 ns duration of laser pulses. Gating the detector to turn on after the laser pulse avoids the detection of the chamber and Rayleigh scattering light, which appears only in the shorter time scale. The operation at reduced pressures should also lead to the slower reaction rate of $O(^1D)$ with H_2O, reducing the laser-generated spurious OH. ii) The usage of the high repetition rate laser as an excitation light source can reduce the interference by the formation of OH through the photolysis of ozone. The OH formation process from ozone requires two photons, one to photolyze and one to excite the resultant OH to the fluorescent state of OH, whereas the ambient OH is excited by only one photon and fluoresces. The spurious/ambient signal ratio can be decreased by decreasing the laser power density. iii) The laser wavelength around 308 nm is used to excite OH radicals to the $v' = 0$ level of the OH $A^2\Sigma^+$ state, instead of the laser wavelength of 282 nm to the $v' = 1$ level. At 308 nm the ozone absorption cross-section is only 4% of that at 282 nm and the $O(^1D)$ quantum yield is 18% smaller. The disadvantage of the usage of 308 nm is the difficulty in isolating the OH fluorescence signal at 308 nm from the chamber and Rayleigh scattering.

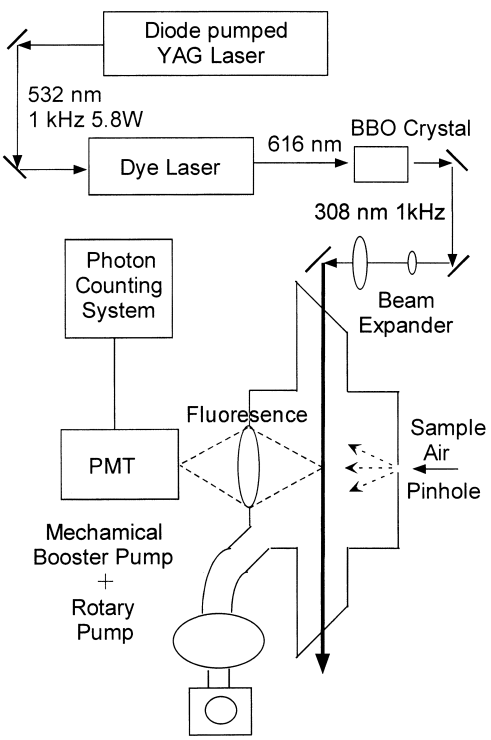

Fig. 1. Schematic diagram of the OH instrument developed in this study.

1. Instrument Description.

A schematic diagram of the LIF instrument is shown in Fig. 1. The instrument consists of i) a laser system to generate the excitation radiation, ii) a LIF cell, iii) a fluorescence detection system, and iv) a data acquisition system.

1-1. Laser System. The combination of a frequency-doubled Nd:YAG laser (Lambda Physik, StarLine) and a tunable dye laser (Lamda Physik, ScanMate 1E) is used as an exciting light source, which is operated at a high repetition rate (1 kHz). The high repetition rate allows for high average laser power with low pulse energy. This avoids the ozone interference and the saturation problem as described before. For the detection of atmospheric OH, some of the groups have been used copper vapor lasers as the excitation source of tunable dye lasers,[7,8,10] due to the high repetition rate up to 10 kHz. In this study, the diode laser pumped YAG laser is used for the dye laser excitation source due to easy operation procedures. The dye solution used for the dye laser is a mixture of Rhodamine 101 and Rhodamine B in methanol solvent. The tunable dye laser light around 616 nm is frequency doubled by a BBO crystal to produce tunable UV light around 308 nm. The 308 nm light is separated from the red fundamental 616-nm light by a prism system. The maximum average laser power produced by this laser system at 308 nm is approximately 150 mW, which corresponds to 150 μJ/pulse. The tunable light around 308 nm has a spectral width of $\sim$0.15 cm^{-1} in fwhm (full width at half maximum). Since this linewidth value almost matches the Doppler width of OH radical at room temperature, high efficiency for the OH excitation can be expected. The pulse duration of the 308-nm light is about 5 ns, which is much shorter than the fluorescence lifetime of the OH radical at a few hundred Pa (200ns–500ns). The power level of the UV laser light is controlled by a neutral density filter, the transmission level of which is in the range of 0.01% to 100 %. The typical power for the ambient OH detection is 10 mW to prevent the saturation of OH absorption and the ozone interference. The wavelength of the laser is controlled by a microcomputer. The angle of the BBO crystal is also controlled by the computer. The laser beam size is expanded by a beam expander lens system in front of the LIF cell to reduce the laser power density. The beam expander consists of $f = 10$ mm and $f = 50$ mm convex lenses. The beam diameter of the UV laser light in the fluorescence cell is about 10 mm. The UV laser power is monitored by a power meter (SCIENTECH, Model S310).

1-2. Laser-Induced Fluorescence Cell. A schematic diagram of the LIF cell and fluorescence detection system is shown in Fig. 2. Ambient air is expanded through a pinhole (diameter 1.0 mm) into the chamber. The fluorescence cell is pumped by a combination of a mechanical booster pump and a rotary pump (ULVAC PMB003 + VD401, 5000 L/min). The pressure in the fluorescence cell is kept at 266 Pa. The pressure in the fluorescence cell is monitored with a capacitance manometer (MKS 122A, full scale 1333 Pa). The volumetric flow rate inside the cell is estimated to be 10 slm (standard liter per minute). The flow rate in the fluorescence cell must be fast enough that the same sampled air is not irradiated with two successive laser pulses, so that OH molecules produced by the first laser pulse through the ozone reactions are not excited by

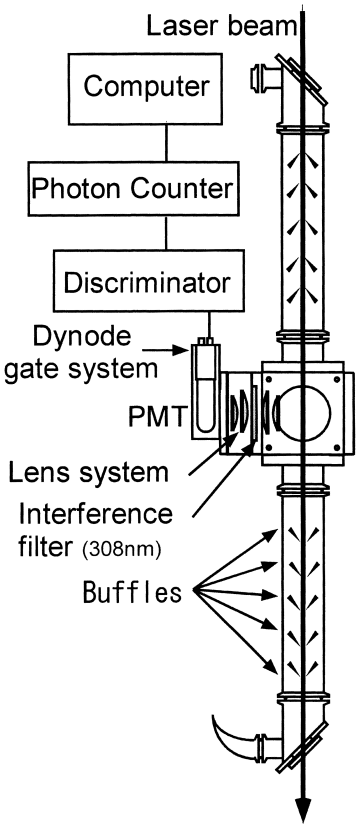

Fig. 2. Schematic of the laser-induced fluorescence cell and detection system.

the second laser pulse. Careful attentions have been paid to reduce the chamber scattering. As shown in Fig. 2, the cone-shaped aperture assemblies with holes of 12–16mm diameter are inserted into the entrance and exit arms. The inner walls of the fluorescence cell were painted with a colloidal carbon to reduce the wall scattering.

The fluorescence from OH radicals is collected by a set of four anti-reflection coated quartz lenses as shown in Fig. 2. The two inner convex lenses have a diameter of 60 mm and a focal length of 100 mm, while the outer two convex lenses have a diameter of 50 mm and a focal length of 100 mm. A narrow-band optical interference filter (Bar Associates) is equipped to detect only the fluorescence from OH at 308 nm and to minimize the detection efficiencies of fluorescence from other species and of sunlight from the outside through the pinhole. The center wavelength of the filter is 312 nm, the maximum transmission coefficient at the peak is about 60%, and the diameter is 70 mm. The performance of the filter is designed for the normal incident angle onto the filter surface. Since the incident angle is critical for the spectral performance of the filter, the interference filter is located between the inner lenses of the fluorescence collection system, where the incident angles onto the filter are close to the normal.

1-3. Fluorescence Detection System. The photomultipliers (PMTs) with a quartz window and a multi- or bi-alkali photocathode are selected so that the OH fluorescence at 308 nm is detected. Various models of PMTs are tested in this study, which are Hamamatsu model R928, R106UH, R212UH, 1P28 and R4332 PMTs. Not only the fluorescence from OH radicals but also the scattering light of the laser pulse hit the PMT photocathode. There are two sources of the laser scattering light, one is internal reflection of the laser light on the walls in the LIF cell, which is called chamber scattering, and the other is Rayleigh scattering from the sample air molecules. The Rayleigh scattering is unavoidable in principle, since it appears at the identical wavelength with the fluorescence. Since the chamber scattering is reduced with the cone-shaped aperture assemblies, its intensity is much smaller than that of Rayleigh scattering in our LIF cell. The time duration of the scattering light is almost identical with that of the laser light itself, which is about 5 ns, while the fluorescence lifetime of OH radicals is about 200 ns under the pressure conditions of 266 Pa. Therefore, the fluorescence signal can be separated from the scattering signal by gating the PMT signal. The gate of the photon counter is opened after the laser pulse duration and for the time range of several hundred ns. The scattering light intensity mainly due to the Rayleigh scattering is much larger than that of OH fluorescence under the practical conditions for OH measurements. If the PMT is kept highly sensitive for the laser pulse duration, the intense scattering light hits the PMT photocathode and saturates the output signal of the PMT. This saturated signal lasts for several hundred ns, which prevents the detection of weak OH fluorescence. A dynode gate circuit for the PMT is used to avoid this saturation effect. By changing the dynode voltage of the PMT with a high voltage pulse gate circuit, the PMT has almost no sensitivity for the laser pulse duration, while it is turned on 50 ns after laser pulses and it has high sensitivity for about 20 μs. The timing of the dynode and counting gate is controlled by a delay generator (Stanford Research, DG535).

1-4. Data Acquisition System. The intensity of the weak fluorescence signal from the PMT is measured using a photon counting technique. The PMT output is fed into a discriminator (Hamamatsu, C3866). The number of pulses after the discriminator is counted by a high-speed counter (Hamamatsu, M3949), which is slotted into a microcomputer (NEC, PC-9821AP). To avoid the switching noise of the dynode gate system, the gate of the photon counter is opened at the timing of 140 ns after laser pulses. The counting gate width is 500 ns.

2. Calibration and Performance of the Instrument.

In an LIF technique, the intensity of the fluorescence is monitored. It is almost impossible to derive an absolute concentration directly from the measured LIF intensity itself, because accurate estimations of the detector efficiency and the fluorescence collection efficiency are difficult. Therefore, the LIF instrument must be calibrated by using a standard sample with a known concentration. However, there is no stable standard gas for OH radicals, since OH radicals are very reactive and their atmospheric lifetime is about 1 s. In this study, two calibration methods are used, one is a long-path absorption technique[6,12] and the other is a titration technique with simultaneous photolysis of water vapor and oxygen.[9,12,13,30,31]

2-1. Calibration with the Long-Path Absorption Technique. The absolute OH concentration can be determined by absorption using Beer's law,

$$[\mathrm{OH}] = \ln(\frac{I_0}{I})L^{-1}\sigma^{-1} \quad (3)$$

where I_0 and I are intensity of the light before and after traversing the absorption path, σ is the integrated absorption cross section for OH, and L is the effective path length. Since the homogeneous concentration of the OH radicals throughout the path length is required, the upper limit of the path length is on the order of a hundred meters even with a multi-pass absorption cell. When the absorbance is measured with the pulsed laser light, the detection limit of the absorbance is few percent due to the pulse-to-pulse fluctuation. Therefore, the minimum density of the OH radicals for the calibration with the absorption technique is about 10^{11} radicals cm^{-3} with the path length of $L = 100$ m. This concentration is much higher than the typical atmospheric OH concentration (10^6 radicals cm^{-3}). Under such a high OH concentration more than 10^{11} radicals cm^{-3}, the photon counting system of our OH instrument is saturated when the laser power is set to the level for the ambient atmospheric detection (10 mW). Therefore, the calibration of the instrument is carried out at the low laser power level of about 0.001 mW.

The absorption cell used in this study for the calibration of the OH instrument has a multi-pass optics which is called a White cell.[32] The White cell consists of one large concave mirror (dia. 100 mm) with entrance and exit cutaways and two small concave mirrors (dia. 50 mm) in the other side. The focal lengths of all the concave mirrors are 0.5 m. The reflectance of the dielectric coating on the mirrors is about 99% for one reflection at 308 nm. The distance between the large mirror and the two small mirrors is 1 m. The UV laser beam for the LIF excitation is also used for the absorption measurements. About half of the laser beam from the laser system is split into the absorption cell. The laser beam passes 100 times in the absorption cell with the multi-pass optics, the effective path length is 100 m. The 100 times reflections on the mirrors reduce the laser beam power to about 30–40% of the initial level even without OH absorption. The intensities of the laser beam at the entrance and exit of the absorption cell are monitored by photodiodes.

The air inlet pinhole to the LIF cell is located just below the multi-passing laser beam. Nitrogen gas with water vapor is flowed into the absorption cell. The pressure in the absorption cell is kept almost equal to atmospheric pressure. OH radicals are produced by the photodissociation of the water vapor with irradiation of a low-pressure Hg lamp at 184.9 nm,

$$\mathrm{H_2O} + h\nu\,(184.9\ \mathrm{nm}) \rightarrow \mathrm{OH} + \mathrm{H} \quad (4)$$

The 1 m long size Hg lamp is used so that the OH concentration in the absorption cell is homogenous. The absorption cell is purged from the outside air so as not to produce ozone molecules which are generated by the photodissociation of oxygen in the air. Since the ozone molecules absorb the laser light at 308 nm, they interfere with the absorption measurements.

Figure 3 illustrates typical absorption and fluorescence spectra obtained simultaneously in the absorption calibration experiment. The upper trace shows the absorption spectrum, while the lower trace shows the LIF excitation spectrum. The horizontal scale represents the laser wavelength, while the vertical scale represents the transmission and LIF intensity for the absorption and LIF spectra, respectively. The strongest peak in the spectra is assigned to the $Q_1(2)$ rotational line of the OH $A^2\Sigma^+\ v' = 0 \leftarrow X^2\Pi_{3/2}\ v'' = 0$ band. The concentration of OH radicals is calculated to be 2.0×10^{11} cm^{-3} from the absorption spectrum, using the line strength and pressure broadening parameters reported by Dorn et al.[22] The relationship among the number of fluorescence photons per second S_{OH}, the corresponding OH concentration [OH], and the laser power I_{p} is given by

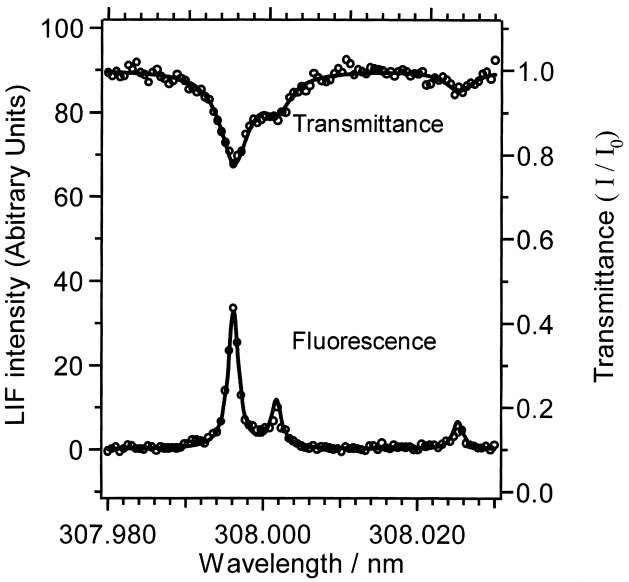

Fig. 3. Absorption spectrum (upper trace) and fluorescence excitation spectrum (lower trace). The horizontal scale is the laser wavelength. The absorption spectrum is measured with the multi-pass absorption cell. The concentration of OH is calculated to be 2.0×10^{11} radicals cm^{-3} from the absorption measurement. The strongest peak in the spectra is assigned to the $Q_1(2)$ rotational line of the OH $A^2\Sigma^+\ v' = 0 \leftarrow X^2\Pi_{3/2}\ v'' = 0$ band.

$$S_{\mathrm{OH}} = C_{\mathrm{OH}}[\mathrm{OH}]I_{\mathrm{p}} \quad (5)$$

where C_{OH} is the sensitivity factor of the instrument. Since the nitrogen is used as a buffer gas instead of the air in this calibration of the long path absorption, the correction for the oxygen quenching effect for ambient measurements is necessary. The sensitivity factor of the OH instrument after the correction for the air buffer conditions is determined to be $C_{\mathrm{OH}} = 2.1\times10^{-7}$ count s^{-1} mW^{-1} (OH cm^{-3})$^{-1}$ when the laser wavelength is fixed at the peak of the $Q_1(2)$ rotational line.

2-2. Calibration with a Titration Technique. The other technique is also used to calibrate the OH instrument at lower OH concentrations, which is the titration technique with simultaneous photolysis of water vapor and oxygen. The gas mixture of synthetic air (21% O_2/N_2) and water vapor is flowed into a quartz tube (25 mmϕ). The pressure in the quartz tube is atmospheric pressure. The mixture gas is irradiated with a pen-ray Hg lamp. The radiation at 184.9 nm from the Hg lamp dissociates both the H_2O and O_2 molecules in the gas mixture.

The photodissociation of the H_2O molecules produces OH radicals. The O atoms produced by the photodissociation of the O_2 molecules are converted to ozone by the three-body reaction with O_2 molecules. The absorption cross section for H_2O is known from laboratory measurements ($\sigma_{H_2O} = 7.22\times10^{-20}$ cm^2) by Creasy et al.[33] and the effective cross section of O_2 for the 185-nm Hg line is reported to be $\sigma_{O_2} = 1.0\times10^{-20}$ cm^2 under the conditions similar to our system.[33] The dew-point hygrometer (General Eastern, Model 1011B) and ozone analyzer (Thermo Electron, Model 49) is used to measure the concentrations of water vapor and ozone, respectively. In the titration technique with simultaneous photolysis of water vapor and oxygen, the concentration of the OH radicals, [OH], is expressed as

$$[OH] = \frac{[O_3][H_2O]\sigma_{H_2O}}{2[O_2]\sigma_{O_2}} \quad (6)$$

Therefore, the concentration of OH radicals can be derived from only the measurements of O_3 and H_2O concentrations. In the present calibration system, the OH concentration is controlled by changing the water vapor mixing ratio. The water vapor mixing ratio was in the range of 200–1000 ppmv, while the O_3 mixing ratio measured was in the range of 3–10 ppbv. Only the small center portion of the laminar airflow from the quartz tube was sampled into the fluorescence cell through the nozzle and the average value of the ozone concentration in the air flow was measured by the ozone analyzer. Taking account of the radial distribution of ozone concentration across the quartz tube, the concentration of O_3 in the center portion was estimated to be twice of the average value.[9]

The typical concentration of OH radicals produced in this system is determined to be 1–3$\times10^9$ radicals cm^{-3} from the O_3 and water measurements. Figure 4 shows the calibration results, where the laser wavelength is fixed at the peak of the $Q_1(2)$ rotational line of the OH $A^2\Sigma^+$ $v' = 0 \leftarrow X^2\Pi_{3/2}$ $v'' = 0$ band. From the calibration experiment shown in Fig. 4, the sensitivity factor of the OH instrument is determined to be C_{OH} = 2.7$\times10^{-7}$ counts s^{-1} mW^{-1} (OH cm^{-3})$^{-1}$. The laser power used in the calibration with the long-path absorption method is 2–3 orders smaller than that with the titration method. The uncertainty of the values for the laser power measurements is estimated to be about 30% between the two calibration procedures. Therefore, the sensitivity factors obtained with the long-path absorption and the titration methods are in good agreement with each other.

2-3. Background Signal. After the improvements of the shape of the baffles and the black coatings of the inner wall of the LIF cell, the background level due to the wall scattering is much smaller than that due to the Rayleigh scattering by the air molecules (N_2 and O_2). The dynode gate circuit and counting gate system are used to avoid the effect of the Rayleigh scattering. However, even with the dynode gating system the Rayleigh scattering signal is still counted as the background signal. When the intense Rayleigh scattering hits the photocathode of the PMT during the off-time of the dynode gate, the photoelectron pulses appeared in the time period a few hundred ns after the gate is opened. This phenomenon is called an after-pulse effect.[34] The after-pulse effect is a main source of the background signal in the OH instrument developed in this study.

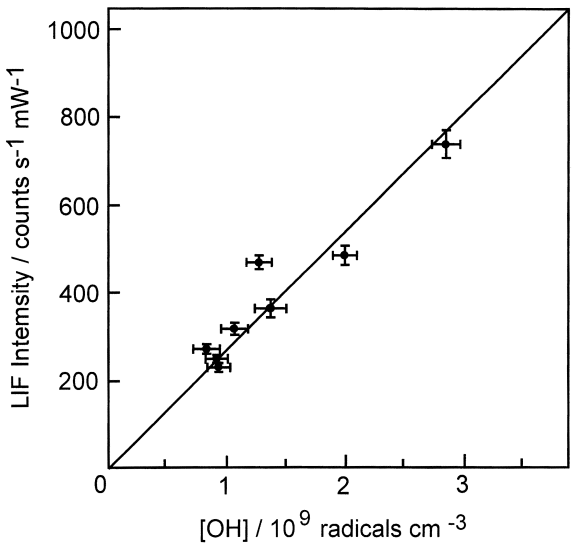

Fig. 4. Calibration plots of the OH instruments using the titration method with simultaneous photolysis of water vapor and ozone, when the laser wavelength is fixed at the peak of the $Q_1(2)$ rotational line. The sensitivity factor for the LIF detection is determined to be 2.7$\times10^{-7}$ count s^{-1} mW^{-1} (OH cm^{-3})$^{-1}$.

The five models of Hamamatsu PMTs (R928, R106UH, R212UH, 1P28, and R4332) are tested in this study, all of which are a type of the side-on. We found that the R928 PMT gives the lowest after-pulse count rate among the PMTs tested.

The two types of the dynode gate circuit are tested in this study. The one is the dynode gate circuit of a commercial socket (Hamamatsu C1392-56), while the other is our homemade circuit for the dynode gate which is normally-off type. The diagram of our home-made dynode gate circuit is shown in Fig. 5. The Hamamatsu circuit controls the voltage of third and fifth dynodes (DY3 and DY5), while the home-made circuit controls the voltage of first, second and fifth dynodes (DY1, DY2 and DY5). The performances of the Hamamatsu and homemade dynode gate circuits are 50 and 5 counts s^{-1} mW^{-1}, respectively, for the background signal due to the after-pulse effects. Therefore, the dynode gate with the home-made circuit in Fig. 5 gives a smaller background signal, which results in the higher sensitivity of the instrument than that with the Hamamatsu gate circuit.

2-4. System Performance. The photon count value due to OH fluorescence, N_{OH} (in counts), is expressed by

$$N_{OH} = C_{OH}\cdot I_p\cdot[OH]\cdot t\,, \quad (7)$$

where I_p is the laser power (in mW), [OH] is the OH concentration in the sample ambient air (in molecule cm^{-3}), t is data accumulation time (in s), and C_{OH} is the detection sensitivity of the instrument per unit laser power (in counts s^{-1} mW^{-1} molecule^{-1} cm^3) when the laser wavelength is tuned at the on-resonance position of the OH rotational line. The detection sensitivity is dependent on the excitation rate at the OH rotational line, on the collection efficiency of the optics and detector, the fraction of OH molecules in the excited state which radiate, and on the density change upon expansion of air into the detec-

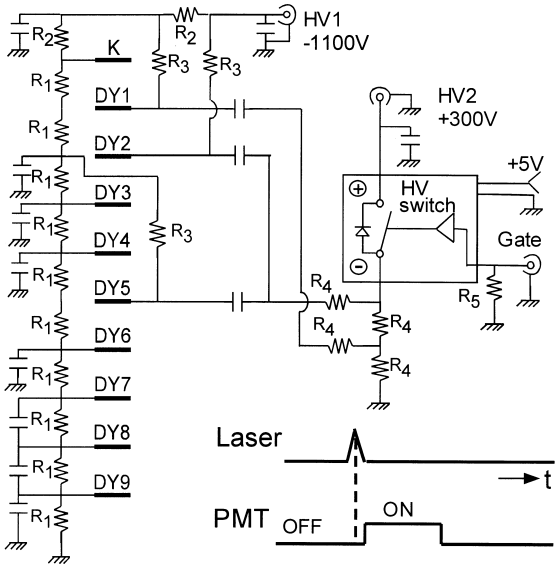

Fig. 5. Circuit diagram of the home-made dynode gate system, which is operated with a normally-off mode. K: photocathode of the photomultiplier (PMT), DY*n*: *n*th dynode of the PMT. R_1 = 330 kΩ, R_2 = 160 kΩ, R_3 = 2 MΩ, R_4 = 100 Ω, and R_5 = 50 Ω. All the capacitances are 10000 pF 2 kV. The high-voltage (HV) switch (Belhke Electronic, HTS-31) is turned on by the positive gate pulse 50 ns after the laser pulse.

tion chamber. The background count value, N_{BG}, is expressed by

$$N_{BG} = S_{BG} \cdot I_p \cdot t, \tag{8}$$

where S_{BG} is the count rate per unit laser power (in counts s^{-1} mW^{-1}) when the laser wavelength is tuned to the off-resonance position. The fluctuation of the laser power is low in our OH system. The detection noise is determined mainly by photon counting statistics near the minimum detection limit, which is expressed by $N^{1/2}$ when the counting value is N according to the Poisson distribution. Therefore, the minimum limit of detectable OH concentration, $[OH]_{min}$, is expressed by

$$[OH]_{min} = \frac{1}{2^{1/2}} \times \frac{S/N}{t^{1/2}} \times \frac{{S_{BG}}^{1/2}}{C_{OH} \cdot {I_P}^{1/2}} \tag{9}$$

where *S*/*N* is a signal-to-noise ratio and t is total data accumulation time. Since the detection time for the [OH] measurement at the on-resonance wavelength is *t*/2 and that for the background at the off-resonance wavelength is *t*/2, the factor $1/2^{1/2}$ appears in Eq. 9. The $[OH]_{min}$ value with the home-made gate circuit is calculated to be 7×10^5 molecules cm^{-3} in accumulation time of 60 s and *S*/*N* = 2.

Discussion

The OH detection system using the LIF technique is constructed and its performance is tested. The minimum detection limit is estimated to be 7×10^5 molecules cm^{-3}. Since this value is very close to typical tropospheric OH concentrations ($\sim1\times10^6$ molecules cm^{-3}), the instrument developed in this study with the LIF and FAGE techniques is useful for tropospheric OH measurements. However, for measurements of atmospheric OH concentrations, the sensitivity of $[OH]_{min}$ = 1–3×10^5 molecules cm^{-3} with an integration time of 60 s is required at least. This means that the OH instrument developed in this study should be improved to have higher sensitivity.

To decrease the minimum detection limit of the OH concentration, the following three points of the improvement are considered: i) increasing the laser power I_p, ii) decreasing the background signal intensity S_{BG}, and iii) increasing the fluorescence collection efficiency to enlarge the C_{OH} value. Since the minimum detection limit is proportional to the inverse of the square root of laser power as indicated in Eq. 9, we can decrease the minimum detection limit by increasing the laser power. However, at a high laser power density, the ozone interference can interfere with accurate OH measurements. Furthermore, the photoabsorption of the OH transition is saturated by the high laser power density, where the population of the ground electronic state of OH is depleted due to absorption of the pump radiation. Therefore, we have to increase the laser power without increasing the laser power density at the LIF cell. Stevens et al.[6] reported that the saturation of the OH transition at the $Q_1(2)$ rotational line is less than 20% when the laser power density is 15 μJ cm^{-2}. In the OH instrument developed in this study, the laser beam diameter is now 10 mm and its density is 13 μJ cm^{-2}. If we extend the beam diameter to 14 mm keeping the same power density, the sensitivity of the system will be 1.4 times higher than the current value.

The minimum detection limit is proportional to the inverse of the fluorescence collection efficiency (see Eq. 9). In the present OH instrument, the side-on type PMT (R928) is used. The size of the photocathode of the R928 PMT is 8×24 mm (1.9 cm^2). PMTs with a larger photocathode are available commercially. For example, the 9816QB PMT made by Electron Tube Company has a photocathode of 46 mm diameter (16.6 cm^2). Since that is a head-on type PMT, a new dynode gate circuit should be designed to reduce the after-pulse effect. To collect fluorescence emitted over wide solid angles and to focus it onto the PMT photocathode, the lens combination of the two 50 mmϕ with f = 100 mm and the two 60 mmϕ with f = 100 mm is used in the present instrument. If we can use a 22% larger diameter lens system with the same focal length, the fluorescence signal will increase 50%. The lens system with the larger diameter and shorter focal length has the larger aberration for the focusing. This implies that a PMT with a large photocathode is required to cover the large focusing spot of the lens system.

The minimum detection limit is also proportional to the square root of the background signal intensity S_{BG} (see Eq. 9). If we can reduce the background signal intensity four times smaller, the minimum detection limit will be a half of the present value. The background level due to the wall scattering is now much smaller than that due to the Rayleigh scattering by the sample air. The dynode gate circuit and counting gate system are used to reduce the effect of the Rayleigh scattering. However, the after-pulse effect is serious in the OH instrument developed in this study. The five models of Hamamtsu PMTs are tested in this study, all of which are the side-on type. It is found that the Hamamatsu R928 PMT gives the lowest after-pulse count rate among the tested PMTs. The photocathode material of the R928 PMT is made of multi-alkali, while those

of the others is bi-alkali. This suggests that multi-alkali photocathode PMTs produce fewer after-pulses than bi-alkali PMTs. The conductivity of the multi-alkali photocathode is much smaller than that of the bi-alkali photocathode. Since it is speculated that the after-pulses effect is caused by charge-up on the photocathode, it is reasonable that the multi-alkali PMT shows less after-pulse effect.

The two types of the dynode gate circuit are tested with the side-on PMT in this study. It is found that the circuits to switch the voltages of the first and second dynodes near the photocathode (DY1, DY2) gives less after-pulse effect than that of the DY3 and DY5 dynodes. The background signal caused by the after-pulse effect is much reduced by the dynode gate circuit of the DY1 and DY2 switching.

Detection of the ambient OH radicals by the laser-induced fluorescence technique can be affected by the ozone interference. The ozone interference is caused by reactions (1) and (2). In the OH instrument developed in this study, the pumping speed in the LIF cell is fast enough that the same volume of the sample air is not irradiated with successive laser pulses. Therefore, the amount of the OH radicals produced by the ozone interference is calculated within the duration of a single laser pulse, and is compared with that of the original atmospheric OH radicals. Zeng et al.[35] estimated the contribution to the ambient OH concentration from the laser generated OH with a master equation model. Their model incorporated the quantum state specific production of OH from the reaction (2) and rotational energy transfer. They predicted that interference from laser generated OH accounts for less than 1% of the total LIF signal, for [OH] = 10^6 molecules cm^{-3}, [O_3] = 5 ppb, 40% relative humidity, and at cell pressure of 27–670 Pa. Since the conditions used in our OH instrument are similar to those used in their model calculations, the ozone interference is negligibly small in our OH instrument.

We thank Drs. H. Akimoto and Y. Kanaya (Frontier Research System for Global Change) and Dr. Y. Kajii (The University of Tokyo) for their helpful advices and discussions. This work was supported by the TOYOTA High-Technology Research Grant Program. The support of this work by Grants-in-Aid for Scientific Research from the Ministry of Education, Culture, Sports, Science and Technology, is also acknowledged.

References

1 B. J. Finlayson-Pitts and J. N. Pitts Jr., "Chemistry of the Upper and Lower Atmosphere: Theory, Experiments, and Applications," Academic Press, San Diego (1999).

2 A. N. Thompson, *J. Atmos. Sci.*, **52**, 3315 (1995).

3 D. H. Ehhalt, *Phys. Chem. Chem. Phys.*, **1**, 5401 (1999).

4 L. Jaeglé, D. J. Jacob, W. H. Brune, and P. O. Wennberg, *Atmos. Environ.*, **35**, 469 (2001).

5 D. R. Crosley, *J. Atmos. Sci.*, **52**, 3299 (1995).

6 P. S. Stevens, J. H. Mather, and W. H. Brune, *J. Geophys. Res.*, **99**, 3543 (1994).

7 F. Holland, M.Hessling, and A. Hofzumahaus, *J. Atmos. Sci.*, **52**, 3393 (1995).

8 M. R. Heal, D. E. Heard, M. J. Pilling, and B. J. Whitalker, *J. Atmos. Sci.*, **52**, 3428 (1995).

9 D. J. Creasey, P. A. Halford-Maw, D. E. Heard, M. J. Pilling, and B. J. Whitaker, *J. Chem. Soc., Faraday Trans.*, **93**, 2907 (1997).

10 J. H. Mather, P. S. Stevens, and W. H. Brune, *J. Geophys. Res.*, **102**, 6427 (1997).

11 K. Tsuji, K. Nakata, H. Oishi, and K. Shibuya, *Bull. Chem. Soc. Jpn.*, **73**, 2695 (2000).

12 Y. Kanaya, Y. Sadanaga, J. Hirokawa, Y. Kajii, and H. Akimoto, *J. Atmos. Chem.*, **38**, 73 (2001).

13 A. Hofzumahaus, U. Aschmutat, M. Meβling, F. Holland, and D. H. Ehhalt, *Geophys. Res. Lett.*, **23**, 2541 (1996).

14 P. S. Stevens, J. H. Mather, W. H. Brune, F. Eisele, D. Tanner, A. Jefferson, C. Cantrell, R. Shetter, S. Sewall, A. Fried, B.Henry, E. Williams, K. Baumann, P. Goldan, and W. Kuster, *J. Geophys. Res.*, **102**, 6379 (1997).

15 F. Holland, U. Aschmutat, M. Hessling, A. Hofzumahaus, and D. H. Ehhalt, *J. Atmos. Chem.*, **31**, 205 (1998).

16 R. D. Mauldin, D. J. Tanner, and F. L. Eisele, *J. Geophys. Res.*, **104**, 5817 (1999).

17 J. P. Abram, D. J. Creasey, D. E. Heard, J. D. Lee, and M. J. Pilling, *Geophys. Res. Lett.*, **27**, 3437 (2000).

18 L. Jaeglé, D. J. Jacob, W. H. Brune, I. Faloona, D. Tan, B. G. Heikes, Y. Kondo, G. W. Sachse, B. Anderson, D. L. Gregory, H. B. Singh, R. Pueschel, G. Ferry, D. R. Blake, and R. E. Shetter, *J. Geophys. Res.*, **105**, 3877 (2000).

19 I. Faloona, D. Tan, W. H. Brune, L. Jaeglé, D. J. Jacob, Y. Kondo, M. Koike, R. Chatfield, R. Pueschel, G. Ferry, G. Sachse, S. Vay, B. Anderson, J. Hannon, and H. Fuelberg, *J. Geophys. Res.*, **105**, 3771 (2000).

20 H.-P. Dorn, U. Brandenburger, T. Brauers, M. Hausmann, and D. H. Ehhalt, *Geophys. Res. Lett.*, **23**, 2537 (1996).

21 W. Armerding, M. Spiekermann, J. Walter, and F. J. Comes, *J. Atmos. Sci.*, **52**, 3381 (1995).

22 H.-P. Dorn, U. Brandenburger, T. Brauers, and M. Hausmann, *J. Atmos. Sci.*, **52**, 3373 (1995).

23 G. H. Mount, J. W. Brault, P. V. Johnston, E. Marovich, R. O. Jakoubek, C. J. Volpe, J. Harder, and J. Olson, *J. Geophys. Res.*, **102**, 6393 (1997).

24 U. Brandenburger, T. Brauers, H.-P. Dorn, M. Hausmann, and D. H. Ehhalt, *J. Atmos. Chem.*, **31**, 181 (1998).

25 F. L. Eisele, D. J. Tanner, C. A. Cantrell, and J. G. Calvert, *J. Geophys. Res*., **101**, 14665 (1996).

26 D. J. Tanner, A. Jefferson, and F. L. Eisele, *J. Geophys. Res.*, **102**, 6415 (1997).

27 C. C. Felton, J. C. Sheppard, and M. J. Campbell, *Environ. Sci. Technol.*, **24**, 1841 (1990).

28 T. M. Hard, C. Y. Chan, and A. A. Mehrabzadeh, *Environ. Sci. Techol.*, **18**, 768 (1984).

29 C. Y. Chan, T, M. Hard, A. A. Mehrabzadeh, L. A. George, and R. J. O'Brien, *J. Geophys. Res.*, **95**, 18569 (1990).

30 M. Schultz, M. Heitlinger, D. Mihelcic, and A. Volz-Thomas, *J. Geophys. Res.*, **100**, 18811 (1995).

31 A. Hofzumahaus, T. Brauers, U. Aschmutat, U. Brandenburger, H.-P. Dorn, M. Hausmann, M., Hessling, F. Holland, C. Plass-Dülmer, M. Sedlacek, M. Weber, and D. H. Ehhalt, *Geophys. Res. Lett.*, **24**, 3039 (1997).

32 J. U. White, *J. Opt. Soc. Am.*, **66**, 411 (1976).

33 D. J. Creasey, D. E. Heard, and J. D. Lee, *Geophys. Res. Lett.*, **27**, 1651 (2000).

34 D. J. Creasey, P. A. Halford-Maw, D. E. Heard, J. E. Spence, and B. J. Whitaker, *Rev. Sci. Instrum.*, **69**, 4068 (1998).

35 G. Zeng, D. E. Heard, M. J. Pilling, and S. H. Robertson, *Geophys. Res. Lett.*, **25**, 4497 (1998).